Progress In Electromagnetics Research B, Vol. 42, 381–403, 2012

MICROWAVE CONTRAST IMAGING OF BREAST TISSUE FROM LOCAL VELOCITY ESTIMATION

J.-F. Deprez[1], M. Sarafianou[2], M. Klemm[2], I. J. Craddock[2], and P. J. Probert-Smith[1, *]

[1]Institute of Biomedical Engineering, Department of Engineering Science, University of Oxford, OX3 1PJ, UK

[2]Centre for Communications Research, Department of Electrical and Electronic Engineering, University of Bristol, UK

Abstract—This paper proposes a new method to display microwave images of breast tissue, based on estimation of local microwave velocity from time of flight measurements. Its computational demands are low compared with tomography. It has two major components: 1) the estimation of the travel time of microwaves across the tissue between a set of antennae using a wavelet decomposition, and 2) the estimation of the microwave velocity field from the set of travel times using a low dimensional set of radial basis functions to model local velocity. The technique is evaluated in 2-D on clinical MR-based numerical breast phantoms incorporated in Finite-Difference Time-Domain simulations. The basis functions, used with a regularisation scheme to improve numerical stability, reduce the dimensionality of the inverse problem for computational efficiency and also to improve the robustness to error in velocity estimation. The results support previously published findings that the wavelet transform is suitable for robust measurement of time of flight even in clinically significant simulations, and shows that the velocity contrast images can be constructed so different regions of breast tissue type can be distinguished. In particular, the presence of a tumour is clearly detected, demonstrating the potential of this approach for breast screening. Keywords: Biomedical signal processing; Microwave imaging; Image reconstruction.

Received 3 May 2012, Accepted 23 July 2012, Scheduled 25 July 2012

* Corresponding author: Penny Probert Smith (penny.smith@eng.ox.ac.uk).

1. INTRODUCTION

Breast cancer represents one in five new cancer cases in women, making it the most frequent cancer among women worldwide [1]. X-ray mammography is currently the gold standard method for breast cancer detection, with ultrasound used in clinic to follow up potential tumours but suffers from several limitations [2, 3] such as high false-positive and false-negative rates, exposure to ionizing radiation, and reduced efficiency when imaging women with radiographically dense breasts. Ultrasound is operator dependent and offers poor tissue contrast.

These limitations have motivated the development of new techniques for breast cancer detection. A promising alternative is microwave imaging [4–6]. The basis for breast microwave imaging is the dielectric contrast between healthy and malignant tissues at microwave frequency [7, 8]. Microwave imaging also avoids the use of ionizing radiation, and could be implemented as a reasonably cheap and portable device.

Image reconstruction follows one of two methods: tomographic reconstruction and radar-based imaging, or some combination of these. In tomography, the goal is to reconstruct the electrical properties of the breast. Inverse scattering approaches using FDTD models have proved most successful in complex images [9, 10] but require multiple processors to achieve a throughput appropriate for clinical use [10, 11]. To address this problem models with reduced dimensionality have been used in the forward path, for example in [9]. In radar based imaging the goal is to create a contrast image of breast tissue, of a type familiar to clinicians through, for example, B-mode ultrasound. Beamforming techniques (for example delay and sum, or more sophisticated techniques to optimise signal to noise ratio such as Capon beamformers) are used to create an image from the backscattered signals, but their performance deteriorates in images with high velocity differences. Tumours may be identified as high scattering regions [12–14].

In this article, we consider a new approach which uses time of arrival of the transmitted signals to derive an image for velocity contrast in the tissue, providing clinical information in a similar format to the B-mode ultrasound image. Following [15, 16] the time of arrival of signals is identified using a wavelet decomposition. Lazaro et al. [16] showed that wavelets were a robust method of matching time domain signals even in a dispersive medium such as breast tissue, as they can handle translated and scaled versions of a waveform. A particular advantage of the method is that it largely avoids the problem of the large skin reflection which is seen in the radar based

approaches [17, 18], but still avoids a solution to the inverse scattering problem, maintaining the lower computational requirements of time of arrival approaches.

A radial basis function network (RBF) is then used to estimate the velocity distribution over the breast. An RBF network reconstructs the image using a low dimensional but continuous model which provides a rapid solution to the inverse problem, and has been applied successfully in fields [9, 19–22], which share with clinical microwave imaging problems of dispersion and high scattering. The linearity inherent in the method ensures that the error surface presents a single minimum (and no local minima) which can be found in a single matrix operation; hence the method is suited well for use in the clinic. The dimension of the model is related to the final resolution required, and for microwave imaging may be kept much lower than the normal grid size used in tomography since there is no need to propagate the forward scattering solution. The method automatically provides interpolation to provide a continuous velocity estimation from a set of imperfect measurements.

The main assumption in the model is that the velocity can be represented by a first order Taylor expansion. Since the purpose of the technique is to provide images for clinicians, quantitative errors resulting from a first order approximation are not important-contrast rather than exact values are needed. The results are displayed in terms of permittivity through an approximate relationship approximation between velocity, to make them easier to compare with the simulations and other methods.

The basis function model of the breast used here differs from [9] in that the basis functions are used to represent velocity and therefore can be related directly to time of flight measurements, rather than being used to represent dielectric properties within a forward scattering framework.

To illustrate and evaluate the method it is tested on 2-D simulations of dense and fatty breasts derived from clinical MR models and taken from the Wisconsin database [23]. This represents a complex and challenging environment, chosen as a clinically significant environment which allows our results to be compared with other methods using the same database (for example [5]). It is significantly more complex than the experiments published using the wavelet method by Lazaro et al. [16]. The system simulated uses a pulse excitation similar to that currently undergoing clinical trials in Bristol Frenchay Hospital [14].

The results presented are preliminary and do not include a fully dispersive model.

2. METHODS

The approach is based on estimating the spatial group velocity distribution $c(X)$ from a collection of microwave travel times across the tissues.

The local velocity in different types of tissue varies with their relative permittivity. For a non-dispersive medium, it depends on the local relative permittivity, $\epsilon_r'(X)$ as follows:

$$c(X) \approx \sqrt{\frac{1}{\mu\epsilon_o\epsilon_r'(X)}} \tag{1}$$

where μ_o is the permeability of free space (and tissue), ϵ_r' the real part of the relative permittivity and ϵ_o the permittivity of free space. Since over the range of frequencies of interest in this paper the variation in velocity with frequency is small [8]. Eq. (1) is a useful approximation, and is used to relate velocity and permittivity in later sections.

The time-of-flight (ToF) between a transmitting antenna Tm and a receiving antenna Rn can be approximated by the integral, along the straight line path between them, of the inverse velocity:

$$\Delta t_{mn} = \int_{Tm}^{Rn} \frac{dl}{c(X)} \tag{2}$$

In the following, we focus on the 2-D problem, i.e., the estimation of the velocity $c(X)$ over a plane. The parameter X is therefore a 2-element vector giving the position in the plane of interest. The equations developed in this section remain valid for the 3-D case.

The method requires an accurate estimation of the travel times between antenna pairs. The technique developed for this purpose is described in the next section. Once these are established, the estimation of the velocity field $c(X)$ becomes an inverse problem, seeking to recover a scalar function from line-integral measurements. A radial basis function (RBF) network, spaced regularly over the tissue region, is used to model the velocity field. Its input is the set of ToF values and its output is a linear combination of basis functions representing local velocity. The magnitude of each function (representing local velocity) can be determined in a single matrix operation, quickly providing an estimate of the microwave velocity distribution (Subsection 2.2).

2.1. Time-of-Flight Estimation

The wavelet transform develops a signal representation based in its similarity to a set of scaled and shifted basis functions, of a single time

limited function, the mother wavelet. The information it contains is related to the frequency content of the signal. It is superior to the Fourier transform for certain types of signal and application in localising the signal in frequency and in time simultaneously. A number of mother wavelets are possible, but since microwave systems typically generate Gaussian-like excitation pulses, a complex Gaussian wavelet was chosen.

For a given signal f and mother wavelet ψ, the continuous wavelet transform at scale a and time τ is defined as:

$$T_f(a,\tau) = \int_{-\infty}^{\infty} f(t)\frac{1}{\sqrt{a}}\psi^*\left(\frac{t-\tau}{a}\right)dt \tag{3}$$

where * is the complex conjugate operator. $T_f(a,\tau)$ can be interpreted as a measure of the match between the signal and a scaled and delayed wavelet, $\psi(t)$.

Estimation of time of flight then requires the signal to be matched between transmitter and receiver. A simple method was used, which estimated the position of the maximum power summed over a set of scales a_k in the pulse received. Using a smaller number of scales in the sum may increase robustness to noise but may lose resolution, and a suitable range of values, a_o to a_1, was chosen empirically. Hence, the time of flight τ_{ToF} can be written as follows:

$$\tau_{\mathrm{ToF}} = arg\max_{\tau}\sum_{k=a_o}^{a_1}\left|T_{f+}(a_k,\tau)\right| \tag{4}$$

Figure 1 shows the real and imaginary parts of the complex Gaussian mother wavelet. Fig. 2 gives an example of a microwave

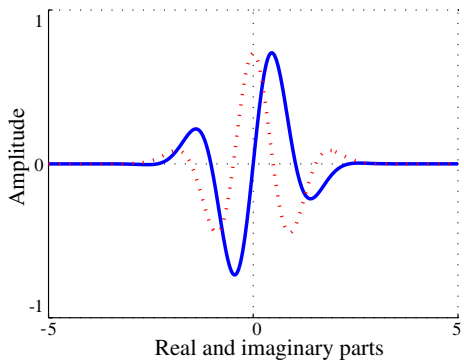

Figure 1. Real (plain line) and imaginary (dotted line) part of the complex Gaussian mother wavelet.

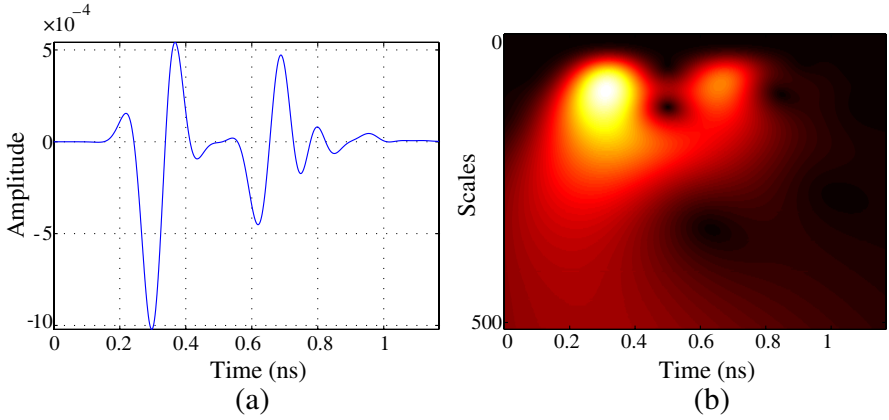

Figure 2. (a) Example of a simulated microwave signal and (b) map of the corresponding wavelet coefficients (absolute value). The x-coordinate of the maximum is used to calculate the ToF between scales $a_o = 30$, $a_1 = 130$.

signal, together with the corresponding wavelet coefficients across scales and time delays.

For use in localising the received signal, Pourvoyeur, et al. [15] used the analytical signals $f^+(t)$ rather than the signal itself $f(t)$:

$$f^+(t) = f(t) + jH\{f(t)\} \tag{5}$$

where $H\{.\}$ is the Hilbert transform operator. This complex extension of the signal was found to increase the robustness and accuracy of the estimation.

2.2. RBF Network: Solution of the Inverse Problem

Assume that the velocity can be represented using a first order Taylor series:

$$c(X) = c_{\text{mean}} + \Delta c(X) \tag{6}$$

where c_{mean} is the mean velocity, determined from the set of ToF estimations, and $\Delta c(X)$ the local fluctuation term to be estimated. Assuming that the fluctuations of the velocity field are small compared to the mean velocity, one can write the inverse:

$$\frac{1}{c(X)} = \frac{1}{c_{\text{mean}} + \Delta c(X)} = \frac{1}{c_{\text{mean}}\left(1 + \frac{\Delta c(X)}{c_{\text{mean}}}\right)} \tag{7}$$

The traversal time Δt_{mn} between two transmit antenna (Tm) and receive antenna (Rn):

$$\Delta t_{mn} = \int_m^n \frac{dl}{c(X)} = \int_m^n \frac{1}{c_{\text{mean}}} \left(1 - \frac{\Delta c(X)}{c_{\text{mean}}}\right) dl \tag{8}$$

and, with some rearrangement:

$$\Delta t_{mn} = \frac{d_{mn}}{c_{\text{mean}}} - \frac{1}{c_{\text{mean}}^2} \int_{Rn}^{Tm} \Delta c(X) dl \tag{9}$$

where d_{mn} is the distance between the transmitter Tm and the receiver Rn. Provided that several line-integral measurements along different directions are available, an estimate of the velocity fluctuation field $\Delta c(X)$ can therefore be reconstructed by inverting this expression.

An RBF network consists of a set of kernels normally placed on regular grid across the image. Each may be specified by its centre position θ_k and weight w_k. The parameter required is then represented by a linear combination of N_f RBFs $f(\theta, k)$ with different weights and centres:

$$\Delta c(X) = \sum_{k=1}^{N_f} w_k f\left(\|X - \theta_k\|\right) \tag{10}$$

where f is a RBF, θ_k and w_k the centre and weight of the kth function, and $||.||$ a norm operator. For computational efficiency, and following [9] it is convenient to choose the RBF as a Gaussian (the most common choice). The norm is taken to be the Euclidean distance:

$$f\left(\|X - \theta_k\|\right) = \exp\left(-\beta \|X - \theta_k\|^2\right) \tag{11}$$

Using Eq. (10) and Eq. (11), Eq. (9) can be written as:

$$\frac{d_{mn}}{c_{\text{mean}}} - \Delta t_{mn} = \frac{1}{c_{\text{mean}}^2} \int_{Tm}^{Rn} \sum_{k=1}^{N_f} w_k \exp\left(-\beta \|X - \theta_k\|^2\right) dl \tag{12}$$

$$= \frac{1}{c_{\text{mean}}^2} \sum_{k=1}^{N_f} w_k \int_{Tm}^{Rn} \exp\left(-\beta \|X - \theta_k\|^2\right) dl \tag{13}$$

In Eq. (13), d_{mn}, the distance between the transmitter Tm and the receiver Rn, can easily be calculated from the geometry of the antenna array. Additionally, the time-of-flight Δt_{mn} between Tm and Rn can be estimated directly from the corresponding microwave signal, as seen in the previous section. As a result, the left hand side of Eq. (13) is known. Three parameters need to be adjusted so the RBF network "fits" the line-integral measurements: the RBF scaling factor β, the

RBF centres θ_k, and the output weights w_k. Once the parameters β and θ_k have been chosen, the inverse problem becomes linear and finding the weights w_k is straightforward. (Note that the choice of the parameters β and θ_k is explained in the next section). Define:

$$u_{mn} = \frac{d_{mn}}{c_{\text{mean}}} - \Delta t_{mn} \tag{14}$$

as the line-integral measurement for the transmitting antenna Tm and receiving antenna Rn,

$$W = \begin{bmatrix} w_1 & w_2 \dots w_{N_f} \end{bmatrix}^T \tag{15}$$

as the vector of weights, and

$$A_{mn} = \frac{1}{c_{\text{mean}}^2} \begin{pmatrix} \int_{Tm}^{Rn} \exp\left(-\beta \left\|X - \theta_1\right\|^2\right) dl \\ \int_{Tm}^{Rn} \exp\left(-\beta \left\|X - \theta_2\right\|^2\right) dl \\ \dots \\ \int_{Tm}^{Rn} \exp\left(-\beta \left\|X - \theta_{N_f}\right\|^2\right) dl \end{pmatrix}^T \tag{16}$$

as the vector of RBF integrals between Tm and Rn. Eq. (13) can be re-written as:

$$u_{mn} = A_{mn} W \tag{17}$$

Or, for all pairs of transmitters and receivers available:

$$U = AW \tag{18}$$

where U is the $N_p \times 1$ vector of line-integral measurements, A is the $N_p \times N_f$ matrix including the RBF integrals, and W is the $N_f \times 1$ vector of weights to be solved. A solution can be found by a least square method:

$$W = \left(A^T A + \lambda I\right)^{-1} A^T U \tag{19}$$

where λ is a regularization parameter used to improve the conditioning of the problem. From the knowledge of the vector W (i.e., the weights w_k of the RBFs), the velocity fluctuation field $\Delta c(X)$ can be reconstructed by Eq. (10), and the velocity distribution is given by Eq. (6). The final step is the reconstruction of the permittivity distribution, which is done through Eq. (1).

3. DESCRIPTION OF THE EXPERIMENTS

3.1. Breast Models

Phantoms from the University of Wisconsin numerical breast phantom repository [23] were used to validate the method. This online database

provides a collection of anatomically realistic numerical breast phantoms derived from series of T1-weighted magnetic resonance (MR) images of healthy patients. Dielectric properties of breast tissues are incorporated in the models from detailed measurements [8, 24]. Each phantom consists of a 3-D grid of cubic voxels, with a spatial resolution of 0.5 mm in each directions.

The data were used within a non-dispersive model to create permittivity and conductivity maps of tissues at 6 GHz. 2-D cross sections on the coronal plane were then extracted and used to run 2-D electromagnetic simulations based on the Finite-Difference Time-Domain (FDTD) method [25].

The phantoms are immersed in a matching medium of relative permittivity $\varepsilon_r = 10$, and include a roughly 1.5-mm-thick skin layer. Since the database does not provide pathological cases, a malignant tumour was simulated by adding to the breast phantoms a homogeneous 6-mm-radius sphere with a relative permittivity of $\varepsilon_r = 50$ [23]. Each phantom is categorized according to the Breast Imaging Reporting and Database System of the American College of Radiology [26], designed to provide a standardized terminology and classification system. For this preliminary study, four different phantoms were used: Model 1: healthy mostly fatty, Model 2: as Model 1 but with simulated tumour, Model 3: scattered fibro-glandular model and Model 4: heterogeneously dense.

3.2. Data Acquisition

A simple antenna array, consisting of 24 point source antennas evenly distributed on the perimeter of a circle, was positioned around the phantom, as shown in Fig. 3(a) (which shows too the dielectric distribution in Model 1). Each antenna was used in turn to transmit and the ToFs found to all other antennas acting as receivers ($N_p(N_p-1)$ ToFs in all). An in-house Finite-Difference Time-Domain (FDTD) code was used to simulate 2-D multistatic microwave measurements, based on the corresponding permittivity and conductivity maps. The antennas were excited with a modulated Gaussian pulse of 6 GHz centre frequency (Fig. 3(c)).

3.3. RBF Network Parameters

To position the RBF centres, a preliminary stage of skin surface reconstruction was performed, using the algorithm developed by Sarafianou, et al. [27]. The RBF centres were automatically and regularly positioned within a perimeter slightly larger than the one defined by the skin reconstruction. This step is not mandatory, and

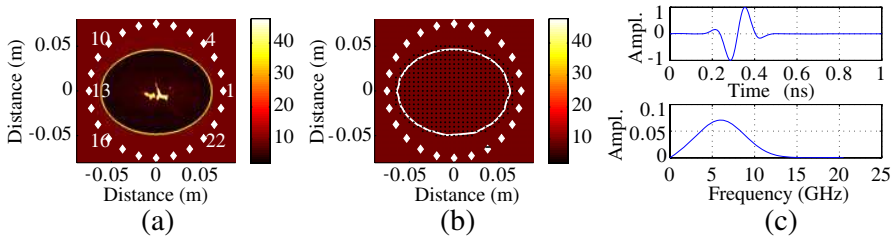

Figure 3. Model 1: (a) Relative permittivity map and positions of the antennas (white diamonds). $\epsilon'_r > 32$: Fibroconnective/glandular tissues. $\epsilon'_r < 7$: Fatty tissue. $7 < \epsilon'_r < 32$: Transitional areas. The skin has $\epsilon'_r = 35$. (b) Positions of the RBF centres (black dots) on 5 mm square grid, and the skin reconstruction (white line); $N_f = 465$. (c) The excitation pulse and its spectrum.

the RBF centres could be placed either regularly or randomly within the perimeter of the antenna array. Fig. 3(b) shows typical positions of the basis function centres.

The other parameter to be initialised is the parameter β, the radius of each RBF. Since the RBF centres are distributed on a regular grid, $1/\beta$ is simply the distance between the RBF centres (4 mm or 5 mm depending on the model), although their placement may be determined more carefully using, for example, the k-nearest neighbours' algorithm [28]. To improve robustness a degree of regularisation was used. The value of the regularization parameter λ was set empirically to $\lambda = 5 \times 10^{-5} \left\| A^T A \right\|$. In addition ToFs which were significantly in error from the estimated mean were discarded as being physically very unlikely.

The value of c_{mean} is chosen using the mean of the velocity estimated from each ToF.

As an example, the relative permittivity ϵ_r map of Model 1 is shown in Fig. 3(a), together with details of the RBF network, skin reconstruction and excitation.

4. RESULTS

4.1. Time-of-flight Estimations

To establish grounds for comparison the travel time between the transmitting antenna m and the receiving antenna n was estimated for every antenna pair using the MR-based permittivity maps. It should be underlined that these ToFs, $\Delta t_{mn,\,\text{ref}}$ which were taken as

Table 1. Mean relative errors in time of flight measurements for the four models.

	Model 1	Model 2	Model 3	Model 4
Wavelet method	1.8%	1.7%	3.5%	5.6%
Correlation	3.7%	4.3%	5.8 %	10.4%

reference, correspond to a straight line path calculation and hence do not necessarily represent the true ToFs, as they do not include microwave propagation phenomena (such as diffraction).

The ToFs were then estimated using the wavelet technique, $\Delta t_{mn,\text{estim}}$. The two sets of ToFs were close, even when the transmitting and receiving antennas were on opposite sides of the breast, although the errors were larger in the highly attenuating fibro-glandular model. Relatively large errors also occur when the path between the transmitting antenna and the receiving antenna is tangential to the skin, probably because this configuration leads to diffraction phenomena. As a measure of precision, the mean relative error was calculated for each phantom as:

$$\frac{1}{(N_p)(N_p-1)} \sum_{m=1}^{N_p} \sum_{n=1,n\neq i}^{N_p} \frac{|\Delta t_{mn,\text{estim}} - \Delta t_{mn,\text{ref}}|}{\Delta t_{mn,\text{ref}}} \tag{20}$$

where $N_p = 24$ is the total number of antenna, $\Delta t_{mn,\text{estim}}$ the estimated ToF for the jth signal, and $\Delta t_{mn,\text{ref}}$ the reference ToF for the signal from transmitter m to receiver n. Table 1 shows the mean relative errors in ToFs in each model and compares them with the equivalent using the traditional correlation method to match the transmitted and received signals.

4.2. Velocity and Permittivity Profiles

Following the ToF estimation step, the RBF network technique was used to reconstruct velocity fields and, using Eq. (1) obtain relative permittivity distributions. Relative permittivity, ϵ'_r, rather than velocity is displayed so the results can be compared more easily with the original images and the data available in the breast phantom repository [23]. Figs. 4–6 compare the variation in ϵ'_r along each of the lines shown in the MR maps from which the simulations are derived, for three of the four phantoms. The profile for Model 1 was similar to that for Model 2, but without the additional high permittivity region of the tumour.

We can first observe that estimations are generally relatively close to the ground truth. In particular, uniform regions of tissue are estimated well. However sharp changes and narrow regions are not identified so successfully; this is because of the smoothing effect of the Gaussian kernels and the relatively sparse spacing (centres placed 5 mm apart). This can be seen especially clearly at the skin and in the low peak values of ϵ_r, for example in Fig. 4 where the general profile within the breast is reproduced well. Values of ϵ_r in uniform regions is estimated well in both Figs. 4 and 5 (and in Model 1).

For the last model (Fig. 6), the main high and low permittivity regions are also detected, although the more highly attenuating dense tissue and varying permittivity profile makes this case more challenging.

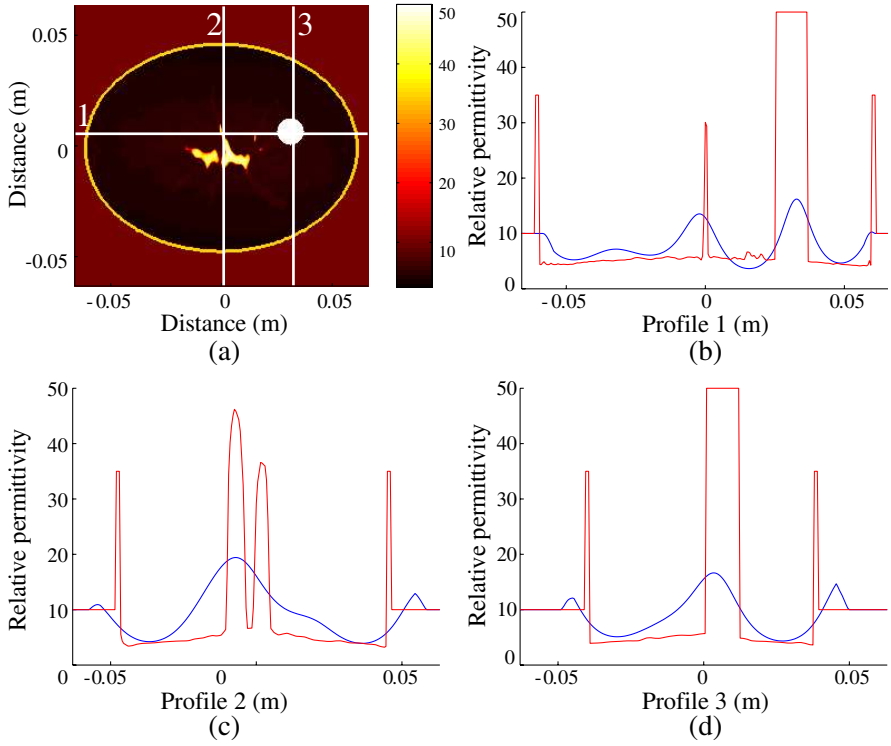

Figure 4. Mostly fatty and pathological model: (a) Ground truth permittivity map (ϵ'_r) and lines showing profiles taken. Estimated (in blue) and ground truth (in red) permittivity ϵ'_r across, (b) profile 1, (c) profile 2, and (d) profile 3.

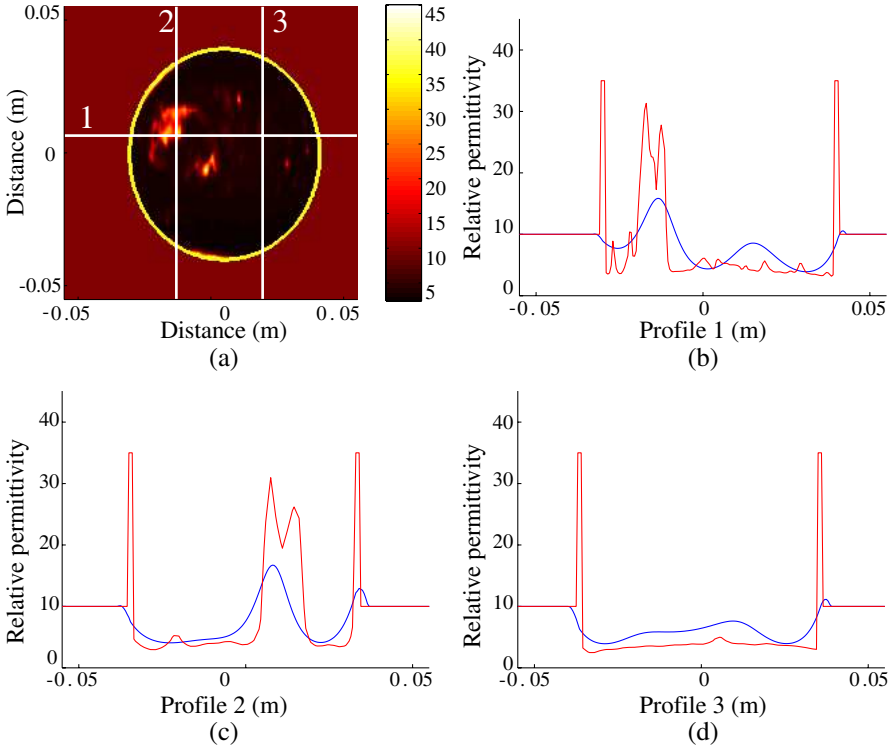

Figure 5. Scattered fibro-glandular model: (a) Ground truth permittivity map (ϵ'_r) and lines showing profiles taken. Estimated (in blue) and ground truth (in red) permittivity ϵ'_r for (b) profile 1, (c) profile 2, and (d) profile 3.

4.3. Permittivity Images

The main purpose of this technique is to provide a qualitative image of the breast which could be of use to clinicians rather than to quantify the local electrical properties. It is clear that the RBFs do not reproduce values faithfully in regions with rapidly changing properties. Again, relative permittivity, ϵ'_r, is shown rather than velocity (using Eq. (1)) to conform with the tissue properties available in the breast phantom repository [23], and to facilitate comparison with other methods. Contrast images are presented in Fig. 7 to Fig. 10, together with the MR maps from which the simulation was derived.

In the first model (Fig. 7), a qualitative image of the centre part of the simulated breast is obtained with the contrast in permittivity clearly illustrated. When a tumour is present (second phantom,

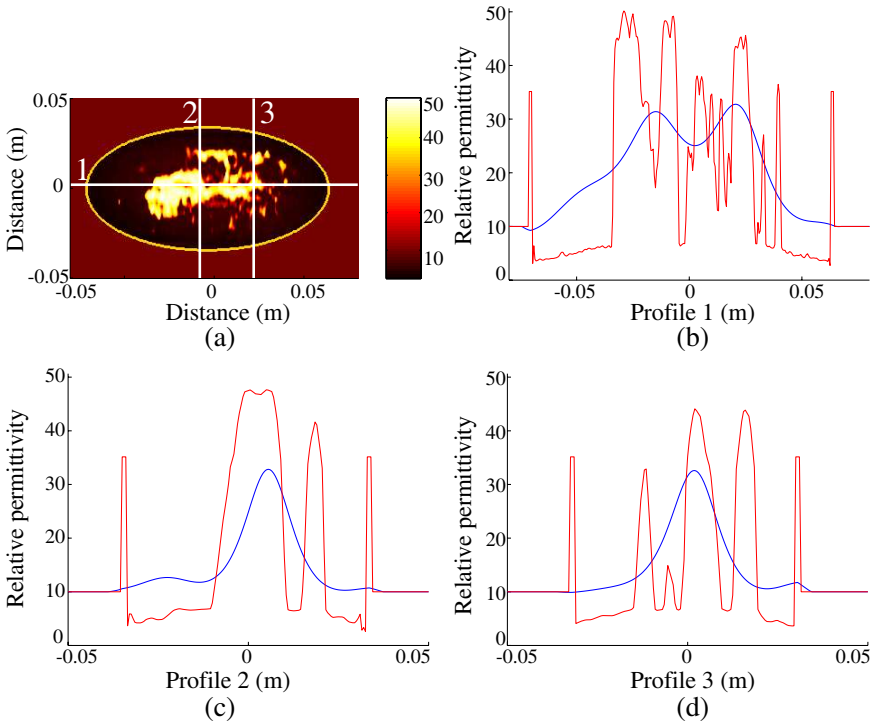

Figure 6. Heterogeneously dense model: (a) Ground truth permittivity map (ϵ'_r) and lines showing profiles taken. Estimated (in blue) and ground truth (in red) permittivity ϵ'_r for (b) profile 1, (c) profile 2, and (d) profile 3.

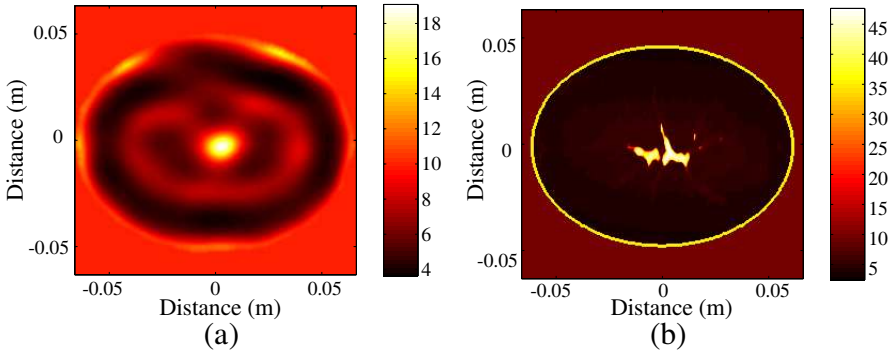

Figure 7. Mostly fatty and healthy model: (a) Estimated ϵ'_r ϵ'_r field and (b) true ϵ'_r field (dB scale).

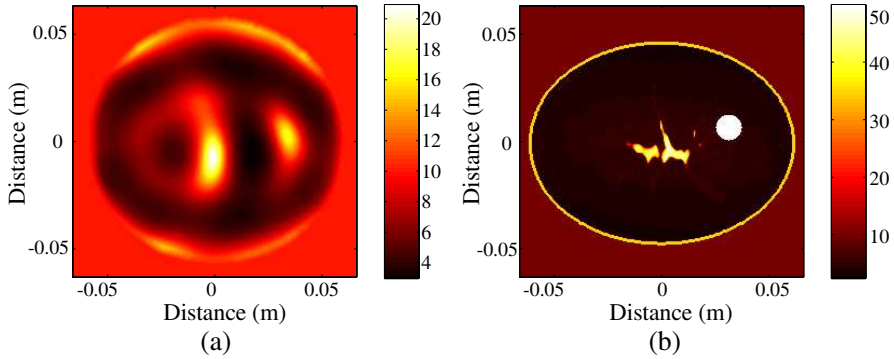

Figure 8. Mostly fatty and pathological model: (a) Estimated ϵ'_r field, and (b) true ϵ'_r field (dB scale).

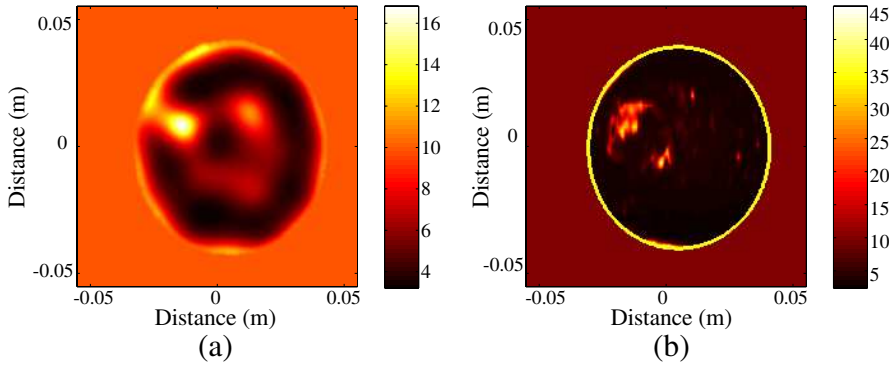

Figure 9. Scattered fibro-glandular model: (a) Estimated ϵ'_r field, and (b) true ϵ'_r field (dB scale).

Fig. 8), the estimation of fatty tissues remains relatively good and the central high permittivity region is still visible. Also, the tumour at 2 o'clock is properly detected since the contrast between the tumour and fatty tissues is significant because of the differences in electrical properties. The fibro-glandular and heterogeneously dense models (Figs. 9 and 10) contains multiple regions of high permittivity (fibro-connective, glandular and transitional tissues). Some of these regions are limited in size and scattered in the tissues, which complicates the estimation. However, the largest regions, at 10 o'clock and in the centre, respectively, are distinguished as well as the fatty tissues.

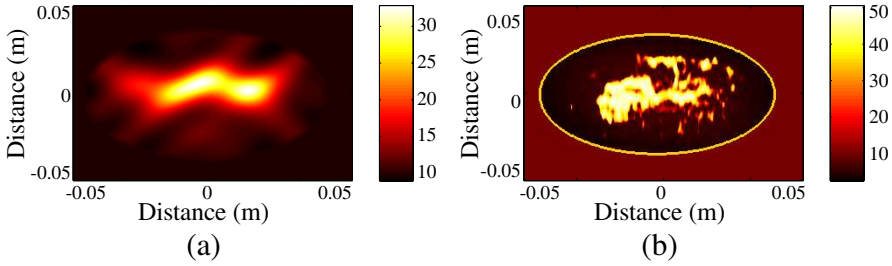

Figure 10. Heterogeneously dense model: (a) Estimated ϵ'_r field, and (b) true ϵ'_r field (dB scale).

4.4. Discussion

A potentially real time method to provide contrast images to assist in tumour detection has been presented. It uses a multi-basis function with an optimisation method based on estimated ToF measurements. Because of the relatively small number of basis functions it does not return the true values of permittivity, especially in regions of rapid tissue variation, but it provides contrast maps which allow regions such as tumours to be identified.

It is assumed that the travel time between a transmitter and a receiver can be formulated as the integral, along the straight line path, of the inverse of the velocity. In fact, since microwave propagation is characterized by phenomena such as diffraction, scattering, or multiple reflections, the path between the transmitter and the receiver is more likely to be a curve. Therefore the straight line integral is only an approximation to the true ToF. This is the case especially for signals travelling tangentially to the breast surface (i.e., when transmit and receive antenna are close). This effect is reduced by averaging across many different signal paths as different antenna are used in turn as the transmitter.

It is also assumed that the differences in velocity across the tissue can be approximated as a first order change on an average velocity. In fact the variation in dielectric constant may be as high as a factor of ten between fatty tissue and malignant tissue [8] and so this assumption may lead to further error in absolute values (the difference is less in denser breast tissue.

The time of flight estimation returns an average velocity, whereas in for real media the velocity will be frequency dependent. The only significance in this for the RBF model is further inaccuracy in absolute values of relative permittivity. However more significant is its effect in time of flight estimation. The two pole Debye model in [8] suggests that

over the frequency range 3–8 GHz (around the 3-dB points in Fig. 3(c)) the change in velocity in tissue is within 3% although the difference in conductivity is larger (up to 16%) (less for very adipose issue). Over a similar frequency range Lazaro et al. [16] suggest that the wavelet transform should be robust to time of flight measurements with dispersion. However modelling of dispersion in the simulated received signals using the 2-pole Debye model and using the predominant tissue type (following [8] suggests that the mean relative errors for the wavelet method in Table 1 become between 2.12% and 7%. Since the method is sensitive to ToF error (as evidenced in the different images in Figs. 4 to 6, some deterioration of the images would be expected (although the error for most tissue types is still lower than that for the non-dispersive simulation in the fibro-glandular case in Fig. 6).

Reconstruction, even using an inverse scattering model, reduces contrast especially for small regions [5]. This effect is seen in all methods and is clear in the results presented in this paper. Quantitatively the effect is seen most clearly in the cross sectional profiles of Figs. 4–6. It is clear that the absolute estimate of permittivity, even in cases in which the variation is low, is reduced by up to about 33%, with peak values even more adversely affected. However since in clinical use the requirement is for contrast imaging rather than a full quantitative reconstruction this is not necessarily a problem; for example B-mode ultrasound has widespread clinical use and presents only contrast information (often quite weak contrast). However of more serious concern is the balance between contrast and size of tumour because of the smoothing effect of the radial basis functions. Although the 12 mm lesion is distinguished in Fig. 5, both this figure and Fig. 6 suggest that the maximum spatial rate change of relative permittivity is limited to around 7 over 1 cm, demonstrating the trade-off between contrast and spatial resolution for tumour detection. Different architectures of the network and different RBFs, such as polyharmonic spline functions, will be investigated to allow more flexibility in the estimation of quick-changing profiles.

For comparison, the results were compared with an inverse scattering solution by Shea et al. using simulations from the same database [5]. As far as can be assessed from the figures (especially Fig. 6 in [5]) the quantitative results are not that different. The underestimate in relative permittivity over large areas is similar although Shea's method gives a better estimate of the true value in regions of rapid variation of permittivity. This is at the expense of a much longer execution time. Shea's model includes a 3-D simulation of data acquired at four frequencies between 1.0 and 2.5 GHz, with 40 offset antenna in five elliptical rings. Although the dispersive effect

over this range of frequency is likely to be small a 3-D model is likely to include greater scattering and hence measurement error, and the number and configuration of antenna also affects the resolution.

A more exact comparison remains to be done through a full simulation. More sophisticated methods to match wavelets in scale space, for example using amplitude or phase matching across the range of coefficients, may give better results. A better approach would be to provide some compensation for dispersion in the signals received. Since the dispersion curve of breast tissue which is less than 84% adipose and malignant tissue was shown by Lazebnik et al. [8] to have similar dispersion characteristics an equalisation filter prior to the wavelet transform stage may be suitable. Other methods might include estimation of the dispersion characteristics within the solution scheme (for example Fang et al. [31] use a first order approximation) or signal decomposition methods [29]. These need to be investigated and a dispersive simulation is being developed.

The most difficult case for breast tumour detection is in fibroglandular (dense) breasts, for which the contrast between background tissue and malignant tissue is low. In [5], Shea suggests that contrast agents, which are preferentially taken up by the tumour, need to be employed in the clinical imaging protocol for women with this type of breast as there is too little contrast even using a full inverse scattering method; other work (e.g., [30]) makes the same point. The method presented in this paper would again be a viable alternative to tomography in providing contrast images.

A major strength of the algorithm lies in its speed, a consideration in clinical use when often high throughput is needed. Producing the estimates of the velocity and permittivity fields shown here took approximately 90 seconds on a single processor (2.8 GHz CPU and 8 GB RAM) running with Matlab. Most of this processing time is dedicated to the wavelet transform (*cwt* function in Matlab) in ToF estimation. Reconstruction of the velocity and permittivity distributions from the ToFs takes only a few seconds. Recent experiments suggest that ToF measurements using only the lower half of scale space produces comparable results, resulting in a reduction in overall execution time of nearly four. Further improvements are possible through using a compiled language such as C++, or by distributing the ToF calculations over a number of processors since the ToF calculation operates independently on each signal with the pulse transmitted. Some increase would be expected for a 3-D measurement since the number of antennas would need to be increased, although ToF calculation could proceed in parallel with data acquisition.

5. CONCLUSION

In this manuscript, we introduced a potentially fast, relative permittivity imaging algorithm for microwave breast imaging. The method is based on a radial basis function network and uses wavelets to estimate the travel times between transmitting and receiving antennas.

A particular feature of the algorithm is its fast execution speed which derives largely from the approximation of the tissue properties by a set of basis functions which required only a sparse set of measurements from the data. In terms of offering fast execution time it is in the same class as the delay and sum beamformer, but without the assumption on uniform velocity to determine spatial position. In addition it is not affected in the same way by the large echo at the skin; a pre-processing step to remove this is not needed. In comparison to tomography its resolution and quantitative estimation is poorer but the speed of execution very much faster.

The algorithm was evaluated on three different classes simulated from MR images of breast tissue. The presence of a tumour, and high permittivity regions such as fibro-glandular tissues, were clearly detected in the reconstructed images. However the dielectric contrast between normal and malignant fibro-glandular tissues is too low for small tumours to be detected. At microwave frequency it may be as low as 10% [8], and as a consequence, pathological tissues do not necessarily differentiate from healthy fibro-glandular tissues. This problem has been reported using other image reconstruction methods as well (e.g., [5]). Recent studies showed that the infusion of a contrast agent which specifically alters the dielectric properties of tumours can significantly improve the tumour detection performances. The method presented here is fully compatible with contrast-enhanced image acquisition.

In a practical 3-D configuration it is unlikely that there would be as many as 24 antenna in each annulus. A practical configuration would take more than one set of acquisitions on a smaller density of antenna, through rotation or lateral movement of the set of antenna between readings. Processing and acquisition could take place in parallel to enhance speed.

While preliminary, these results demonstrated that the new algorithm offers an interesting alternative to microwave imaging and radar-based imaging, and that it may be a promising tool for breast screening especially when high throughput is needed. However two important extensions need to be made to the simulated FDTD models to test the algorithm more fully. The first is to include dispersion as discussed previously. The second is to extend the 2-D simulation into

3-D: this does not affect the methodology significantly but is likely to introduce more artefacts through the greater scattering which will occur.

ACKNOWLEDGMENT

This work was supported by the Engineering and Physical Sciences Research Council (EPSRC, United Kingdom) under the grant "EP/G003335/1 — Enhanced UWB Radar Imaging of Breast Tumours."

REFERENCES

1. International Agency for Research on Cancer, World Cancer Report, June 2008, http://www.iarc.fr/en/publications/pdfs-online/wcr/2008/wcr_2008.pdf.
2. Fletcher, S. W. and J. G. Elmore, "Mammographic screening for breast cancer," *New England Journal of Medicine*, Vol. 37, 1672–1680, 2003.
3. Nelson, H. D., K. Tyne, A. Naik, C. Bougatsos, B. K. Chan, and L. Humphrey, "Screening for breast cancer: An update for the U.S. preventive services task force," *Annals of Internal Medicine*, Vol. 151, No. 10, 716–726, 2009.
4. Meaney, P. M., M. W. Fanning, T. Raynolds, C. J. Fox, Q. Fang, C. A. Kogel, S. P. Poplack, and K. D. Paulsen, "Initial clinical experience with microwave breast imaging in women with normal mammography," *Academic Radiology*, Vol. 14, 207–218, 2007.
5. Shea, J. D., P. Kosmas, B. D. Van Veen, and S. C. Hagness, "Contrast-enhanced microwave imaging of breast tumours: A computational study using 3-D realistic numerical phantoms" *Inverse Problems*, Vol. 26, 1–22, 2010.
6. Klemm, M., I. J. Craddock, J. A. Leendertz, A. W. Preece, D. R. Gibbins, M. Shere, and R. Benjamin, "Clinical trials of a UWB imaging radar for breast cancer detection," *European Conference on Antennas and Propagation (EuCAP)*, 1–4, Barcelona, Spain, 2010.
7. Gabriel, S., R. W. Lau, and C. Gabriel, "The dielectric properties of biological tissues: II. Measurements on the frequency range 10 Hz to 20 GHz," *Phys. Med. Biol.*, Vol. 41, 2251–2269, 1996.
8. Lazebnik, M., D. Popovic, L. McCartney, C. B. Watkins, M. J. Lindstrom, J. Harter, S. Sewall, T. Ogilvie, A. Magliocco, T. M. Breslin, W. Temple, D. Mew, J. H. Booske, M. Okoniewski,

and S. C. Hagness, "A large-scale study of the ultrawideband microwave dielectric properties of normal, benign and malignant breast tissues obtained from cancer surgeries," *Physics in Medicine and Biology*, Vol. 52, 6093–6115, 2007.

9. Winters, D. W., J. D. Shea, P. Kosmas, B. D. Van Veen, and S. C. Hagness, "Three-dimensional microwave breast imaging: Dispersive dielectric property estimation using patient-specific basis functions," *IEEE Trans. Med. Imaging*, Vol. 28, 969–981, 2009.
10. Fang, Q., P. M. Meaney, and K. D. Paulsen, "Viable three-dimensional microwave imaging: Theory and numerical experiments," *IEEE Trans. Antennas and Propagation*, Vol. 58, 449–458, 2010.
11. Golnabi, A. H., P. M. Meaney, N. R. Epstein, and K. D. Paulsen, "Microwave imaging for breast cancer detection: Advances in three dimensional image reconstruction," *Annual International Conference of the IEEE Engineering in Medicine and Biology Society, EMBC*, 5730–5733, Prague, 2011.
12. Li, X., E. J. Bond, B. D. Van Veen, and S. C. Hagness, "An overview of the ultra-wideband microwave imaging via space-time beamforming for early-stage breast-cancer detection," *IEEE Antennas and Propagation Magazine*, Vol. 47, No. 1, February 2005.
13. Kurrant, D. J., E. C. Fear, and D. T. Westwick, "Tumour response estimation in radar-based microwave breast cancer detection," *IEEE Trans. Biomed. Eng.*, Vol. 55, 2801–2811, 2008.
14. Klemm, M., I. Craddock, J. Leendertz, A. Preece, and R. Benjamin, "Radar-based breast cancer detection using a hemispherical antenna array — Experimental results," *IEEE Trans. on Antennas and Propagation*, Vol. 57, 1692–1704, 2009.
15. Pourvoyeur, K., A. Stelzer, G. Ossberger, T. Buchegger, and M. Pichler, "Wavelet-based impulse reconstruction in UWB-radar," *IEEE Int. Symp. on Microwave Theory and Technology*, 603–606, 2003.
16. Lazaro, A., D. G. Firbau, and R. Villarino, "Wavelet based breast tumour localization technique using a UWB radar," *Progress In Electromagnetics Research*, Vol. 98, 75–95, 2009.
17. Deprez, J.-F., M. Klemm, P. P. Smith, and I. J. Craddock, "Twin target correction for ultra-wideband radar imaging of breast tumours," *IEEE International Symposium in Biomedical Imaging*, 213–216, 2010.
18. Fear, E. C., X. Li, S. C. Hagness, and M. A. Stuchly, "Confocal

microwave imaging for breast cancer detection: Localization of tumors in three dimensions," *IEEE Trans. Biomed. Eng.*, Vol. 49, 812–822, 2002.

19. Moody, J. and C. J. Darken, "Fast learning in networks of locally tuned processing units," *Neural Computation*, Vol. 1, 281–294, 1989.
20. Jovanovic, I., L. Sbaiz, and M. Vitterli, "Acoustic tomography method for measuring temperature and wind velocity," *IEEE Int. Conf. on Acoustics, Speech and Signal Processing*, Vol. 4, 1141–1144, 2006.
21. Wiens, T., "Sensing of turbulent flows using real-time acoustic tomography," *19th Biennial Conf. of the New Zealand Acoustical Society*, 2008.
22. Deprez, J.-F., M. Sarafianou, M. Klemm, I. J. Craddock, and P. P. Smith, "Breast imaging through microwave velocity reconstruction preliminary results," *Asia Pacific Microwave Conf.*, 2011.
23. University of Wisconsin Computational Electromagnetics Laboratory, UWCEM Numerical Breast Phantom Repository, http://uwcem.ece.wisc.edu.
24. Klemm, M., J. Leendertz, D. Gibbins, I. J. Craddock, A. Preece, and R. Benjamin, "Towards contrast enhanced breast imaging using ultra-wideband microwave radar system," *IEEE Radio and Wireless Symposium*, 516–519, New Orleans, USA, 2010.
25. Yee, K., "Numerical solution of initial boundary value problems involving Maxwell's equations in isotropic media," *IEEE Trans. on Antennas and Propagation*, Vol. 14, 302–307, 1966.
26. American College of Radiology, Breast Imaging Reporting and Database System (BI-RADS), http://www.acr.org/SecondaryMainMenuCategories/quality_safety/.
27. Sarafianou, M., D. R. Gibbins, I. J. Craddock, M. Klemm, J. A. Leendertz, A. Preece, and R. Benjamin, "Breast surface reconstruction algorithm for a multi-static radar-based breast imaging system," *Europ. Conf. on Antennas and Propagation*, 1–5, 2010.
28. Duda, R. O., P. E. Hart, and D. G. Stork, *Pattern Classification*, 2nd Edition, Wiley Interscience, NY, 2000.
29. Yavuz, M. E. and F. L. Teixeira, "Full time-domain DORT for ultrawideband electromagnetic fields in dispersive, random inhomogeneous media," *IEEE Trans. on Antennas and Propagation*, Vol. 54, No. 8, 2305–2315, 2006.

30. Chen, Y., I. J. Craddock, and P. Kosmas, "Feasibility study of lesion classification via contrast-agent-aided UWB breast imaging," *IEEE Trans. on Biomedical Engineering*, Vol. 57, No. 5, 1003–1007, 2010.
31. Fang, Q., P. M. Meaney, and K. D. Paulsen, "Microwave image reconstruction of tissue property dispersion characteristics utilizing multiple-frequency information," *IEEE Transactions on Microwave Theory and Techniques*, Vol. 52, No. 8, 1866–1875, August 2004.